Journal of Zhejiang University-SCIENCE A (Applied Physics & Engineering)
ISSN 1673-565X (Print); ISSN 1862-1775 (Online)
www.jzus.zju.edu.cn; link.springer.com
E-mail: jzus_a@zju.edu.cn

Effect of thermo-oxidation on the dynamical and physical properties of ethylene-propylene-diene monomer elastomer*

Ya-jian WANG[1,2], Yu-you YANG[†‡1], Lin-bing WANG[2,3]

[1]*School of Engineering and Technology, China University of Geosciences (Beijing), Beijing 100083, China*

[2]*Joint USTB-Virginia Tech Lab on Multifunctional Materials, USTB, Beijing 100083, China*

[3]*Department of Civil and Environmental Engineering, Virginia Tech, Blacksburg, VA 24061, USA*

[†]E-mail: yangyuyou@cugb.edu.cn

Received July 16, 2020; Revision accepted Nov. 19, 2020; Crosschecked June 30, 2021

Abstract: Understanding the underlying processes associated with the thermo-oxidative performance of the ethylene-propylene-diene monomer (EPDM) is essential for assessing and improving its waterproofing performance in underground infrastructures. To explore the fundamentals of EPDM degradation behavior during thermal oxidation, this paper investigates the effects of hydrocarbon free chain, carbon crosslink, chain scission, hydroxyl, and ether crosslinks, on its kinetics and mechanical properties through molecular dynamics (MD) simulations. Several EPDM thermo-oxidative models were built and verified by comparing the simulation results of oxygen diffusivity, glass transition temperature, and mechanical properties with reported experimental ones. Then the radius of gyration, free volume, density, transport, glass transition, and uniaxial compression performance were investigated via MD simulations. The results show that crosslinking in the thermal oxidation process has a significant influence on the free volume, glass transition temperature, and mechanical properties of the system; the hydroxyl and chain scission mainly interfere with the transport properties; all of these affect the structural conformation.

Key words: Ethylene-propylene-diene monomer (EPDM) elastomer; Thermo-oxidation; Glass transition temperature; Free volume; Crosslinking

https://doi.org/10.1631/jzus.A2000312 **CLC number:** U454

1 Introduction

Ethylene-propylene-diene monomer (EPDM) rubber, a copolymer with excellent resistance to thermo-oxidation ageing, outstanding weathering ability, nil electrical conductivity, and low permanent deformation, has been used in a wide range of industrial applications, such as garden hoses, washers, roofing membranes, electrical insulation, asphalt modifier, waterproof joint sealing materials for subway tunnels, pipelines, and underpasses (Gorur et al., 1989; Paroli et al., 1991; Moreno and Gorur, 2001; Schurch, 2006; Cui et al., 2012; Ghasemi and Morteza, 2013; Parameswaranpillai et al., 2019a, 2019b). Especially as a waterproof sealing material for underground infrastructure, the oxidation resistance of EPDM plays a major role in its long-term performance. Oxidation of EPDM during service often leads to performance degradation. For example, the hardening of EPDM rubber makes it less flexible and more prone to cracking and results in leakage (Wu et al., 2014; Liu and Zhou, 2016). Therefore, it is important to understand the underlying processes associated with the thermo-oxidation of EPDM to improve its performance or to study targeted repair measures.

Some early studies on the oxidation (thermal or photo-induced) of EPDM were primarily concerned with changes in its physical properties during

‡ Corresponding author

* Project supported by the National Key Research and Development Program of China (No. 2017YFC0805008)

ORCID: Ya-jian WANG, https://orcid.org/0000-0002-5255-4449

degradation. Landi and Easterbrook (1978) focused on the chemical rheology of peroxide-cured EPDM polymers. The termonomer including dicyclopentadiene (DCPD), 5-ethylidene-2-norbornene (ENB), or 1,4-hexadiene (HD) was measured to further study the relationship between the crosslinks formed during oxidation and chain scissions. Scoponi et al. (1994) studied the photooxidation mechanism of three EPDM terpolymers containing different amounts of ENB. Delor-Jestin et al. (2000) carried out photo-ageing, natural ageing, and thermal ageing of EPDM rubber designed for automotive applications, and described the two phenomena involving elastomeric ageing (oxidation and crosslinking) by infrared spectroscopy, dynamic mechanical thermal analysis (DMTA), and tensile testing analysis. Lucas et al. (2002) studied the thermal photooxidation crosslinking reaction of EPDM by refractometry and X-ray diffraction. The change in the soluble fraction of the elastomer caused by oxidation was obtained by refractometry, and the change in crystallinity during oxidation was monitored by X-ray diffraction. Assink et al. (2002) proposed a nuclear magnetic resonance (NMR) relaxation time as a method for monitoring the degradation of the polymer. The EPDM was aged in an oven at 140 °C and was characterized by conventional mechanical and solution measurements.

There are other previous studies that focus on the mechanisms that account for the main routes of EPDM degradation, and help understanding of the fundamental process of oxidation more clearly (Rivaton et al., 2004, 2006; Colin et al., 2019). The thermo-oxidation of EPDM is a radical chain reaction process, which mainly includes chain initiation, chain growth, and chain termination (Choi et al., 2010). In the chain initiation phase, induced by heat, light, or radiation, the most unstable chemical bond of EPDM breaks to form macromolecular free radicals (R·). During the chain growth phase, free radicals combine with oxygen in the air to form peroxy radicals (ROO·), and then further capture the unstable hydrogen atoms with the polymer to produce hydroperoxides and scissions at an early stage (Assink et al., 2002; Wang and Qu, 2003; Tomer et al., 2007). The chain termination phase is dominated mainly by a crosslinking reaction which generates ethers and also forms unsaturated carboxylic acids, ketones, and saturated alcohols (Delor et al., 1998). Additionally, at higher temperatures, with a higher degree of oxidation, free radicals are mainly decomposed into 60% hydroxyl groups and to lesser extent 10% carbonyl groups (Teissedre et al., 1996). Redline et al. (2017) had a similar conclusion that the oxidation of EPDM exposed to thermo-oxidative and hydrolytic ageing is not very strong near 1715 cm^{-1} (carbonyl absorption peak). The effects on physical properties and changes in chemical groups during oxidation have been extensively studied and confirmed. However, few studies have focused on the effects of molecular microstructural changes on dynamic and mechanical properties during oxidation. Therefore, this study aims, through molecular dynamics (MD) simulation, to reveal the microscopic aspects associated with the thermo-oxidation of EPDM and their effect on dynamic and mechanical properties.

Several MD simulations of properties such as transport, free volume, structure, molecular motion, glass transition, and mechanics of polymers have been reported in the literature. Wu and Xu (2006, 2007) established an epoxy resin crosslinking model to study the diffusion behavior of water in epoxy resin. Rutherford et al. (2007) employed MD and grand canonical Monte Carlo (GCMC) modules to monitor the diffusion and dissolution of gases such as helium, hydrogen, and oxygen through EPDM. Ma et al. (2013) used MD simulation to explore the thermal conductivity of EPDM networks. Through MD simulations, Wang et al. (2018) studied the effects of carbonyl, scissions, and crosslinks on the microscopic and macroscopic properties of EPDM. Wang YJ et al. (2019) revealed free volume characteristics related to the viscosity of EPDM and its dependence on temperature, stress, and strain by MD simulations.

In this paper, MD simulation is used to study the effect of thermo-oxidation on the dynamical and mechanical characteristics of EPDM, particularly the effects of crosslinking, chain scission, and oxidation on the glass transition temperature (T_g), free volume, molecular transport, and uniaxial compression properties during degradation. This paper is organized as follows: (1) the main path of thermal oxygen ageing of the EPDM backbone is derived based on bond order calculation results and previous literature; (2) five EPDM molecules are established and placed into amorphous cells in different ratios to form nine models representing different thermal oxidation

stages; (3) the established EPDM MD models are verified by comparison with the experimental results of the thermal (glass transition temperature), mechanical (stress-strain relationship), and transport (gas diffusivity) properties reported in the literature; (4) the validated EPDM model is used to further study the radius of gyration, free volume, density, oxygen diffusion and self-diffusion, glass transition temperature, and uniaxial compression mechanical properties of different thermal oxidation stages.

2 Molecular dynamics simulation of thermo-oxidation in ethylene-propylene-diene monomer

MD simulations were adopted to investigate the kinetic, thermal, and mechanical properties of EPDM at different thermal oxidation stages. Five EPDM molecules, including free chains, carbon crosslinks (C-C), alcohols (OH), chain scissions, and ether crosslinks (C-O-C), were established and mixed in different ratios to form nine EPDM thermal oxidation MD models. Then these models were validated by comparing the calculations of oxygen diffusivity, glass transition temperature, and uniaxial compression curve with the experimental results in the literature.

2.1 Molecular dynamics simulation models

2.1.1 Potentials

The interaction potential function of each particle (molecule or atom) in the system and its related parameters are its force field. Selecting the appropriate force field is important for different simulation systems if reasonable simulation results are to be obtained. Generally, the force field can be expressed as

$$\begin{aligned} E_{\text{total}} &= E_{\text{vdW}} + E_{\text{Coul}} + E_{\text{bond}} \\ &\quad + E_{\text{angle}} + E_{\text{dihedral}} + E_{\text{invert}} + E_{\text{cross}}, \end{aligned} \tag{1}$$

where E_{total} is the total potential energy of the system, E_{vdW} represents the potential energy caused by intermolecular forces, E_{Coul} represents the Coulomb electrostatic potential energy, E_{bond} represents the extension energy of the chemical bonds, E_{angle} represents the angular potential energy of the chemical bonds, E_{dihedral} represents the dihedral rotational potential energy of molecules, E_{invert} represents the vibrational potential energy away from the plane, and the last term, E_{cross}, is the crossover term.

The COMPASS force field was applied to molecular simulations to obtain the vapor pressure, as implemented in the molecular simulation software Material Studio. Using the functional form of CFF-type force fields has been successfully applied in MD simulations of condensed phases. The potential function of the COMPASS force field is expressed in the following form:

$$\begin{aligned} U = &\sum_{ij} \varepsilon_{ij} \left[2\left(\frac{\sigma_{ij}}{r_{ij}}\right)^9 - 3\left(\frac{\sigma_{ij}}{r_{ij}}\right)^6 \right] + \sum_{\text{elec}} \frac{q_i q_j}{r_{ij}} \\ &+ \sum_{\text{bonds}} k_b \left(b - b_0\right)^2 + \sum_{\text{angles}} k_\theta \left(\theta - \theta_0\right)^2 \\ &+ \sum_{\text{dihedral}} k_\varphi \left(1 - \cos(n\varphi)\right), \ n \geq 0, \end{aligned} \tag{2}$$

where the subscripts ij and elec of the summation symbols denote the non-bonded potentials of van der Waals and Coulomb, respectively; bonds, angles, and dihedral denote the bonded potentials; b_0 and θ_0 are the equilibrium bond distance (b) and angle value (θ), respectively, and k_b, k_θ, and k_φ are force constants. The cut-off distance between atoms i and j is denoted by r_{ij}, the potential energy parameter is denoted by ε_{ij}, the finite distance at which the inter-molecular potential becomes zero is σ_{ij}, and q_i and q_j are the fixed partial charges of atoms i and j, respectively, within the same molecule.

2.1.2 Main chain reaction path of thermal oxidation

It is necessary to understand the thermo-oxidative process of EPDM to model it. The presence of the third monomer, ENB, increases the efficiency of the vulcanization, while the sensitivity of ENB also causes oxidation to begin from it, eventually reaching the ethylene-propylene unit (Bouguedad et al., 2008). However, in actual production, the ENB monomer is present at a low content (about less than 9%) (Delor et al., 1998), and it is pointed out in the literature that the reaction rate on the main chain ethylene-propylene

and the reaction rate on the side chain ENB are in the ratio of 9:1 (Zachary et al., 2008). Therefore, the oxidation of the low amount of ENB, which mainly produces some ketones and carboxylic acids, is neglected. Only the oxidation reaction on the main chain of EPDM is considered in this research.

The Mayer bond order is calculated via Dmol3 to determine the location of the most unstable bonds. The bond order is a parameter that reflects the strength of interatomic forces, and the smallest bond level means it is the easiest to react. As shown in Fig. 1, the bond order of tertiary hydrogen on the EPDM main chain is the smallest, which is 0.832 (circled in Fig. 1). This agrees with the literature (Li et al., 2004). The bond at this position is the most prone to be broken to form free radicals.

Degradation is initiated by thermal breakage of the carbon-hydrogen and carbon-carbon bonds along the backbone to produce unstable EPDM radicals (EPDM·). These radicals are susceptible to oxygen to form peroxyl radicals, EPDM (EPDM-OO·). Once the peroxyl radicals are formed, they will capture the unstable hydrogen atom from another polymer molecule and form peroxides (EPDM-OOH) and another carbon radical (EPDM·), thereby forming a repeating cycle. These peroxides are readily further broken down into two free radicals: an alkoxy group (EPDM-O·) and a hydroxyl group (HO·), and the subsequent process becomes autocatalytic. The alkoxy groups and carbon radicals formed by these cyclic reactions will eventually achieve stability. Their possible reaction pathways are shown in Fig. 2. Some couple to each other to complete further ether crosslinking (Duek et al., 1990; Guzzo and de Paoli, 1992) (path 1), or some undergo disproportionation reactions that result in chain scission (path 2) whilst some combine with hydroxyl groups to form alcohols (path 3) (Ferradino, 2003).

2.1.3 MD simulation models

According to the actual production ratio of EPDM (Zachary et al., 2008), ethylene, propylene, and the ENB third monomer are copolymerized in a ratio of 5:4:1, and then five types of EPDM molecules are constructed in the degradation process. As shown in Fig. 3, these five EPDM molecules are hydrocarbon free chain (HFC), carbon crosslinking (CCL), chain scission (CS), hydroxyl chain (HC), and ether crosslinking (ECL) and are denoted by E1, E2, E3, E4, and E5, respectively.

These molecular segments were then mixed in different ratios to build nine amorphous cells with a density of 0.87 g/cm^3 at temperature of 293 K. This was followed by the minimization of the potential energy of the polymer system through a 5000-step geometry optimization calculation, and then a dynamical calculation of 200 ps for NPT, NVT, and NVE was performed successively, with the aid of the

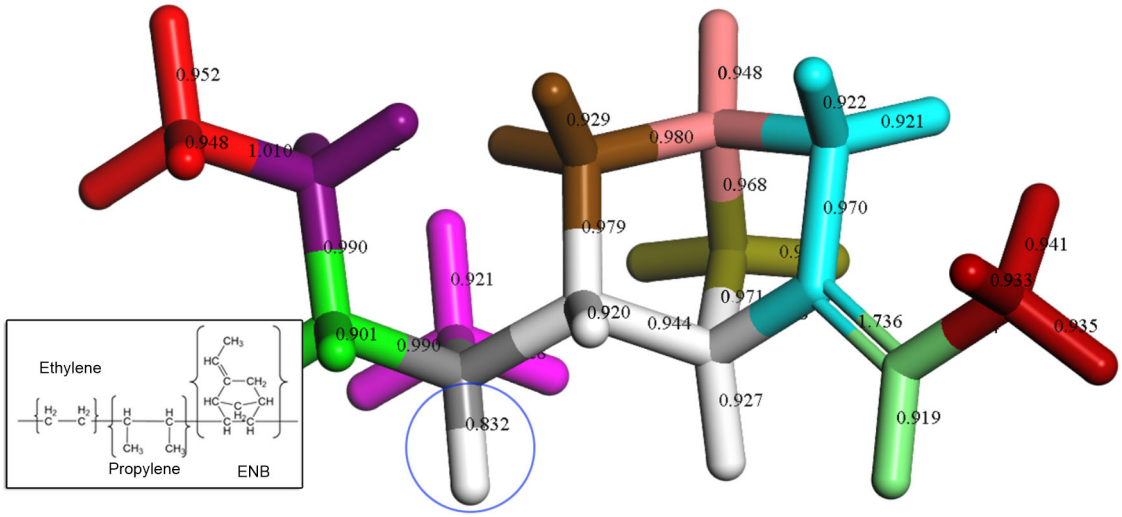

Fig. 1 Quantum chemical calculation results of the EPDM bond order

The minimum bond order is located at the tertiary hydrogen position on propylene and marked with a circle. The inset shows the chemical formula of EPDM

Andersen thermostat and the Berendsen barostat. The letter N represents a constant number of atoms, and P, V, T, E correspond respectively to constant pressure, volume, temperature, and energy in the system in run equilibrium. The energy evolution of the dynamic equilibrium process is illustrated in Fig. 4.

The combination scheme is given in Table 1. M1, M2, and M3 represent the unaged EPDM with different degrees of crosslinking, from which the influence of the number of crosslinking and free chains on the dynamics and mechanical properties can be determined. According to Table 1, M4, M5, and M6 all contain nearly 50% carbon crosslinking, the other half of M4 and M5 are alcohol and chain scission, respectively, and the rest of M6 consists of quarter chain scission and quarter alcohol. These models can be considered as EPDMs in the early stages of oxidation, from which variation in properties caused by hydroxyl groups and chain scission can be investigated. M7, M8, and M9 were established to compare with the above models to investigate the effects of ether crosslinks on EPDM's macroscopic and microscopic properties.

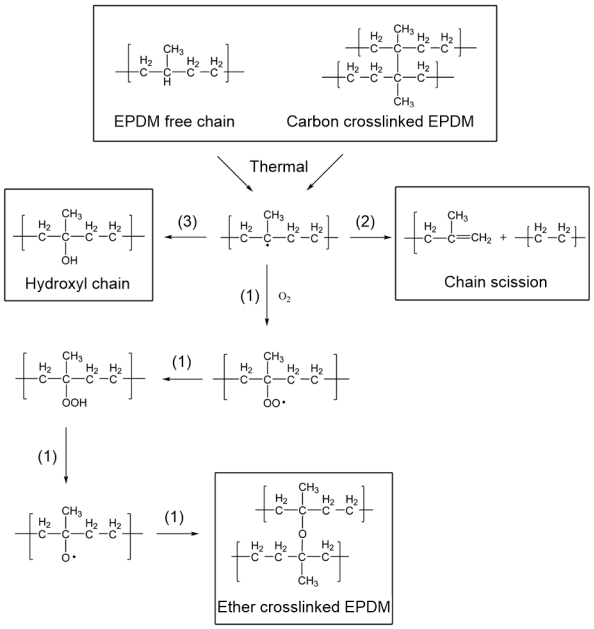

Fig. 2 Possible thermo-oxidative reaction paths of EPDM main chain

Path 1 is a crosslinking reaction in which alkoxy groups and carbon groups are combined, path 2 is a disproportionation reaction leading to chain scission, and path 3 is a combination of a carbon group and a hydroxyl group to form an alcohol

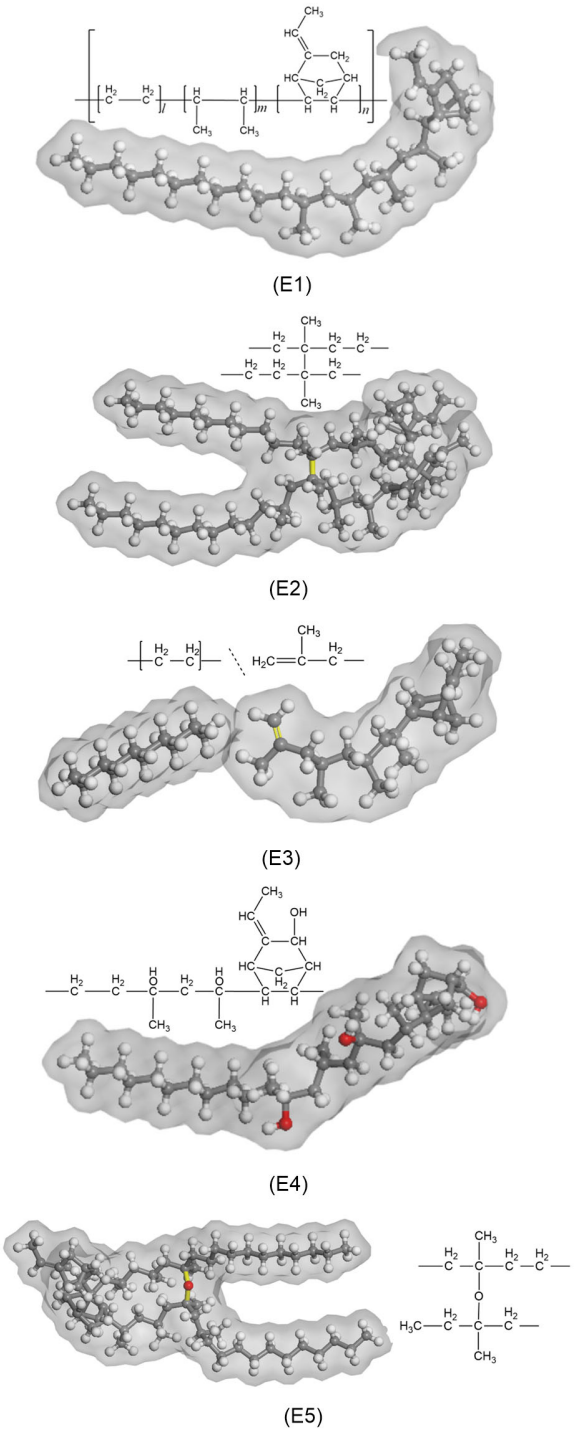

Fig. 3 Unoxidized and oxidized EPDM molecular chains

The carbon atoms are displayed in gray, the hydrogen atoms are shown in white, the oxygen atoms are shown in red, and the crosslinks are shown in yellow. E1 is an uncrosslinked EPDM, E2 is a crosslinked EPDM, E3 is an EPDM scission with C=C, E4 is an alcohol with a hydroxyl group, and E5 is an ether crosslinked EPDM. References to color refer to the online version of this figure

Table 1 Composition and numbering of thermo-oxidative MD models of EPDM, with the netmasses of each EPDM molecule

EPDM molecule	Molecular type	Netmass	Number of chains								
			M1	M2	M3	M4	M5	M6	M7	M8	M9
E1	Hydrocarbon free chain	430.805	40	20							
E2	Carbon crosslinking	859.594		10	20	10	10	10		10	
E3	Chain scission	416.778					20	10	10		
E4	Hydroxyl chain	462.803				20		10	10		
E5	Ether crosslink	875.593							10	10	20

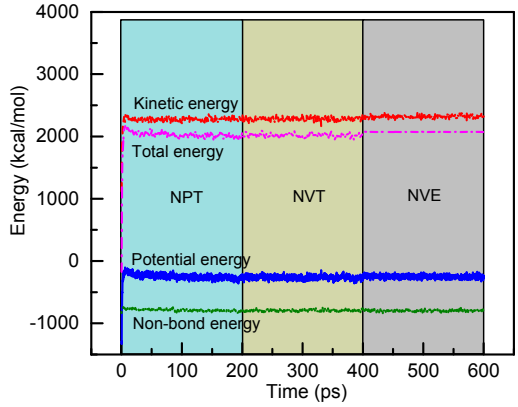

Fig. 4 Energy of M1 for 200-ps NPT, 200-ps NVT, and 200-ps NVE MD simulations

2.2 Molecular dynamic calculation method

2.2.1 Radius of gyration

The radius of gyration can indicate the looseness and free volume of the system. It is the vector distance from the center of mass in the polymer to each chain and can be expressed as

$$\left\langle \boldsymbol{R}_{\mathrm{g}}^2 \right\rangle = \frac{\sum_i m_i r_i^2}{\sum_i m_i}, \tag{3}$$

where $\langle\ \rangle$ indicates statistical average, m_i represents the mass of the ith molecular chain, and r_i represents the distance from the ith molecular chain to the center of mass.

2.2.2 Free volume

Free volume is an inherent defect of polymer materials, and includes atomic-scale and molecular-scale pores between molecular chains, and structural defects caused by random packing of molecular chains. It controls the mobility of molecules and reflects the inherent time-scale and viscosity of materials.

When performing free volume calculations, the MD model is divided into several grids with a spacing of 0.15 Å (1 Å=0.1 nm) by a scanning probe of radius 1 Å. If more than half of the space of the grid is occupied by the probe, it is marked as accessible, and if more than half of the space of the grid is occupied by atoms, it is marked as occupied. The free volume is formed when two accessible cells are arranged in adjacent positions, and the ratio of the free volume to the total volume is the fractional free volume (FFV) (Madkour, 2000).

2.2.3 Diffusion

The relationship between continuous displacement and time can be obtained from the trajectory information of MD simulation atomic diffusion by solving Newton's equation of motion. Then the gas diffusion coefficient can be obtained by calculating the mean square displacement (MSD) of the diffused gas. The diffusion coefficient is calculated by the Einstein equation (Charati and Stern, 1998):

$$D_\alpha = \frac{1}{6N} \lim_{t\to\infty} \frac{\mathrm{d}}{\mathrm{d}t} \sum_{i=1}^{N} \left\langle \left[r_i(t) - r_i(0) \right]^2 \right\rangle, \tag{4}$$

where N is the number of diffusing atoms in the system. $r_i(t)$ denotes the position of the atom at time t and $r_i(0)$ represents the initial position of the atom. The differential of Eq. (4) can be approximated to the ratio of MSD to time differential, that is, the slope of the linear fit curve for MSD, which is denoted as a. Since the calculation result of MSD has averaged the number of diffusion atoms N, Eq. (4) can be approximately simplified to

$$D_\alpha = \frac{a}{6}. \tag{5}$$

2.2.4 Glass transition temperature

The molecular segment of the glassy polymer is almost frozen, and its specific volume increases linearly with increasing temperature, where the specific volume can be derived from the calculations of the free volume described in Section 2.2.2. When approaching the glass transition stage, the segmental motion of the polymer gradually increases, and there is a significant turning point in the relationship between volume and temperature. Usually, the glass transition temperature can be achieved by extending the two fitting curves. It is the temperature at their intersection.

2.2.5 Stress-strain

The equilibrium method can simulate all the elastic constants at a constant temperature (canonical ensemble) and constant energy (microcanonical ensemble). However, it requires a long calculation time to ensure accuracy. The non-equilibrium method provides convenience by directly applying pressure to the system and monitoring strain. This research applies several finite stresses, and measures the resulting strains while accounting for entropy changes in order to obtain the elastic constants of the building models. This can be achieved by the pressure control scheme of Parrinello-Rahman or the Souza-Martins barostat, under which the length and angle of atomic bonds or molecular chain segments are allowed to fluctuate to a certain degree to create strain (Wang YH et al., 2019).

2.3 Model validation

The glass transition is the inherent property of amorphous polymer materials, the stress-strain is the macroscopic property of the molecular structure, and the gas diffusion is the macroscopic manifestation of the molecular motion mode. Reasonable simulation results of those are of great significance in validating the reliability of the model.

The diffusion of oxygen in the EPDM thermal oxidation model was simulated here via NVT for 2000 ps; the glass transition temperature was obtained by a series of NPT MD simulations at temperatures of 148, 178, 208, 238, 268, 298, 333, 363, and 393 K for 1000 ps; the stress-strain relationship was calculated under a stress magnitude of 0–60 GPa. All these results are compared with experimental results to verify the validity of the MD models.

2.3.1 Oxygen diffusivity

Both M2 and M5 contain carbon crosslinks and no oxygen, which is closer to the original EPDM rubber. Therefore, the diffusivity of oxygen in M2 and M5 is selected to verify the model with experiments. As shown in Fig. 5, the diffusivity of oxygen in M2 and M5 is between the results of the simulation and the experiment reported in the literature (Rutherford et al., 2007). This lack of accuracy may be explained by the limited simulation scale and duration (Lim et al., 2007).

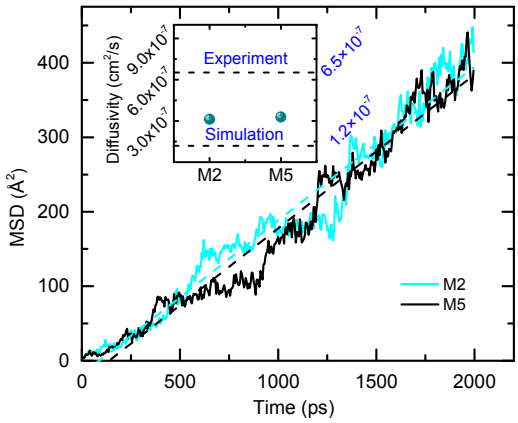

Fig. 5 MSD and diffusivity of oxygen in the M2 and M5 models

The dashed lines are the linear fits of the MSD curves, respectively

2.3.2 Glass transition temperature

Fig. 6a shows the mechanical relaxation spectrum of EPDM reported in (Cao et al., 2016), in which the first peak is called α-relaxation and is thought to be caused by the glass transition. Fig. 6b shows the specific volume fit lines of M1, M2, and M3 at different temperatures. Simulated glass transition temperatures of M1, M2, and M3 are 238, 249, and 255 K, respectively, which agree with the temperature of α-relaxation and are also close to the reported values: 230–250 K (Banik and Bhowmick, 2000; Gu et al., 2015).

2.3.3 Stress-strain

As can be seen in Fig. 7, the slope of the stress-strain curve of the M3 representing original and that of the M8 representing late thermal oxidation almost coincide, and the slopes of M4 and M7 representing the middle stage of thermal oxidation are

smaller than those of M3 and M8. It means that the modulus of the EPDM decreases in the initial oxidation phase and almost rises to the original in the subsequent oxidation phase. The same result can be observed in the experiment (Jiang et al., 2017): the slope of the red curve (thermal-oxidation at 100 °C) in the inset is smaller than the original one, but the slope of the blue curve (thermal-oxidation at 200 °C) is increased to almost coincide with the black curve. Such an agreement can verify the validity of the thermo-oxidative MD models.

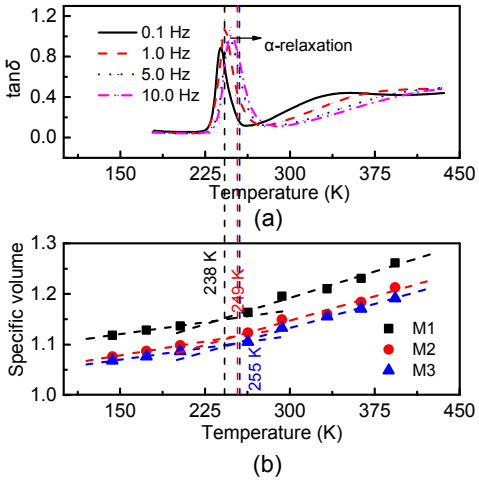

Fig. 6 Glass transition temperature of EPDM

(a) Relaxation curves of 0.1, 1.0, 5.0, and 10.0 Hz at temperatures of 183 to 438 K (δ is the phase angle); (b) Simulation results were the average of the three independent NPT simulations for 1000 ps at temperatures of 148, 178, 208, 268, 298, 333, 363, and 393 K

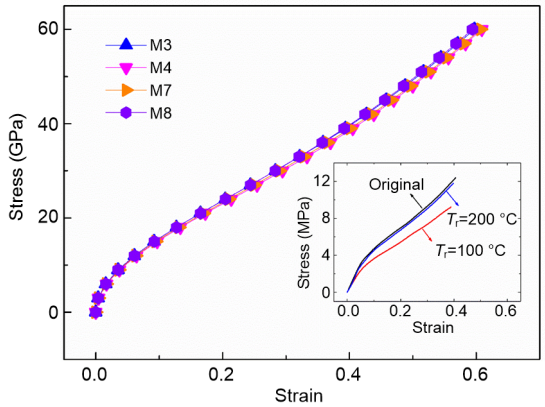

Fig. 7 Uniaxial compressive stress-strain relationship of M3, M4, M7, and M8

The inset in the figure (Jiang et al., 2017) is the test results of the uniaxial compressive stress-strain curve of EPDM after thermal oxidation at different temperatures. References to color refer to the online version of this figure

3 Results and discussion

A series of EPDM thermal oxidation models consisting of free chains, carbon crosslinks, chain scissions, alcohols, and ether crosslinks were built to understand the fundamentals associated with the structure, kinetic, and mechanical properties during degradation. The MD model of EPDM was verified by comparing it with the experimental results for oxygen diffusivity, glass transition temperature, and the stress-strain relationship in the literature. Then the properties of EPDM, such as the radius of gyration, free volume, density, transport, glass transition, and uniaxial stress-strain were derived from the kinetic performance of these models.

3.1 Volume characteristics

3.1.1 Radical radius

As shown in Fig. 8a, the radii of gyration of M3, M8, and M9 are at a high level because they have the same number of crosslinks. This can be verified from Fig. 8b, where carbon crosslinks (C-C) and ether crosslinks (C-O-C) cause a large radius of gyration, mainly around 6–8 Å. There are some differences between the radius of gyration caused by carbon crosslinking and that caused by ether crosslinking. The peak of carbon crosslinking is higher but the distribution is narrower in M3 and M8, while the distribution of the ether crosslinking is wider, which leads to the largest radius of gyration in M9, followed by M8 and M3. M2 and M4 have more carbon crosslinks than M1, so their radii of gyration are larger than that of M1. The radius of gyration of M4 is smaller than that of M2 because the radius of gyration caused by the hydroxyl group in M4 (around 4–5 Å) is smaller than that caused by the hydrocarbon group in M2 (around 5–6 Å). The only difference between M6 and M7 is the type of crosslinks, so they have a similar radius of gyration. M5 has the smallest radius of gyration which is attributed to more chain scissions, mainly distributed around 3–4 Å.

3.1.2 Free volume

In Fig. 9, the occupied volumes of M3, M8, and M9 are small because they have a lot of crosslinks making the connection of the segments compact, while M1 has the largest occupied volume because the components are all free chains. Also, carbon

crosslinks or ether crosslinks in M3, M8, and M9 cause large gyration radii, which result in a large free volume. The carbon crosslinking in M6 shapes a larger radius of gyration than the ether crosslinking in M7, so the free volume of M6 is larger than that of M7. Similarly, the hydroxyl group in M4 shapes a larger radius of gyration than the hydrocarbon group in M5, and the free volume of M4 is larger than that of M5. The occupied volumes of M2, M4, M5, M6, and M7 are almost identical because they have the same number of crosslinks.

In summary, the free volume of the polymer system depends on its radius of gyration, and the volume occupied depends mainly on the degree of crosslinking.

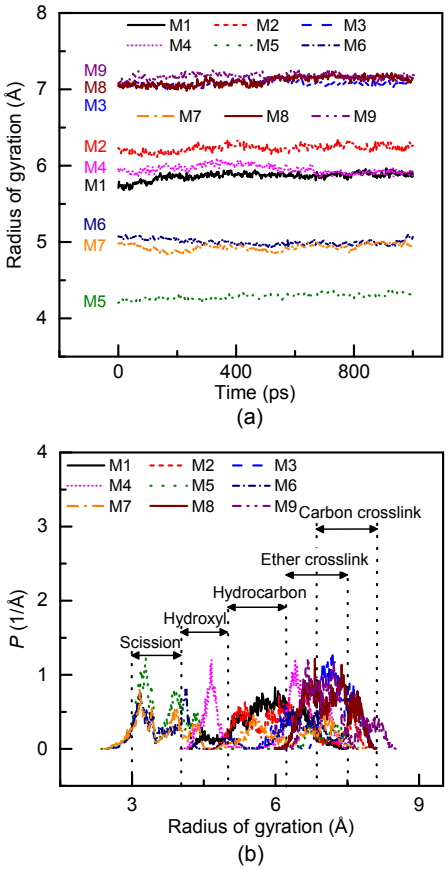

Fig. 8 Evolution and distribution of EPDM radius of gyration

(a) Radical radius of thermal oxygen models running NPT for 1000 ps; (b) Distribution of the radius of gyration. The chemical group causing the distribution is indicated according to the analysis of the differences in the chemical group and the radius of gyration in each system

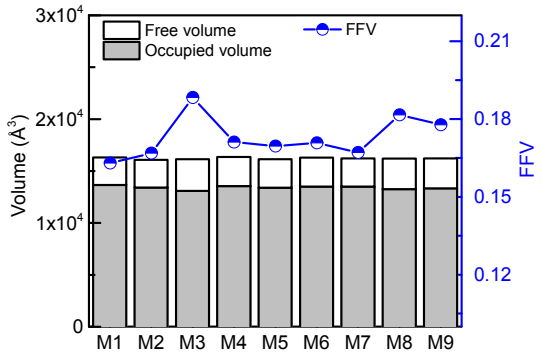

Fig. 9 Free volume and occupied volume of the thermally oxidized MD model

3.1.3 Density

As shown in Fig. 10, the M4 with most hydroxyls, M7 with 50% hydroxyls and 50% ether crosslinks, M3 with 100% carbon crosslinks, and M9 with 100% ether crosslinks are denser, due to volume condensation caused by crosslinking and molecular weight increase caused by oxidation. M6 and M8 are less dense than the above models because less oxygen is present. There are lots of free chains and little oxygen in M1 and M5, which makes them large in volume and light in weight, resulting in low density, while M2 has fewer free chains than either, so its density is greater.

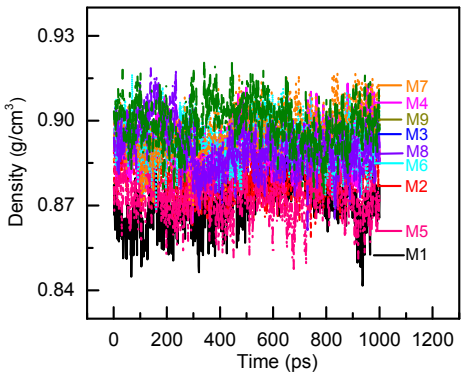

Fig. 10 Density evolution of EPDM thermo-oxidative MD models running NPT for 1000 ps

3.2 Diffusion

3.2.1 Oxygen diffusion

As shown in Fig. 11, initially, oxygen has a rapid transfer in M1. This is because M1 is composed entirely of free chains and there is thus small constraint between molecular chains and loose structures and

molecular chains move fast and easily, eventually leading to rapid oxygen diffusion. In contrast, half the components in M2 and M5 are crosslinked EPDM, resulting in a slower oxygen diffusion. Moreover, the MSD of oxygen in M2 and M5 is longer than that of M1 because half the components of the former two are free chains and the other half are crosslinked, which presents a non-uniform force field in the system, further driving long distance oxygen diffusion. In addition, chain scissions in M5 make the structure looser and the force field distribution different, so that the diffusivity of oxygen in M5 is larger than that in M2. The component of M3 is all crosslinked chains, which leads to a reduction in structural pores, a decrease in molecular thermal motion, and a lack of polarity, further resulting in lower diffusivity than in M2. M4, M6, M7, M8, and M9 contain oxygen, which causes the difference in density of oxygen in the system to be small, and as a result, their oxygen diffusivities are also small. In particular, M4 contains the most hydroxyl groups and so its diffusion rate of oxygen is the smallest. The same reason causes the diffusivity of oxygen in M7 to be greater than that in M6. The diffusivity of oxygen in M8 is, however, greater than that in M7 and M9. It can be inferred that the reaction rate in the late stage of thermal oxidation is slower than the initial because the diffusion of oxygen slows.

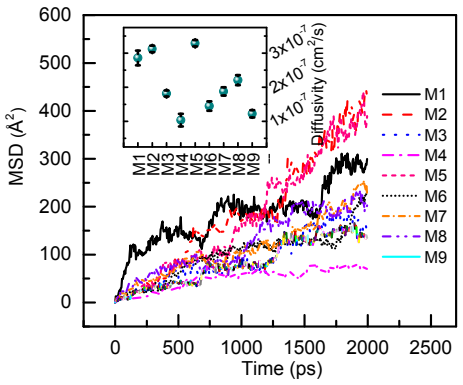

Fig. 11 Diffusion of oxygen in each EPDM MD model
The inset is the average of three calculation results of diffusivity, and the cursor is the maximum error of the calculation results

3.2.2 Self-diffusion

The self-diffusion of molecular chains monitors the relaxation of EPDM. As shown in Fig. 12a, the diffusivity of molecular chain E1 in M1 is greater than that in M2, since M1 has no crosslinks. Fig. 12b shows that the diffusivity of E2 in M5 and M6 is greater than that in M2, M3, M4, and M8 since there are more free chains (scissions) in M5 and M6. The diffusivity of E2 in M2, M4, and M8 is almost at the same level and is larger than that in M3, because there is another kind of molecular chain in them in addition to E2, which causes the concentration difference to facilitate diffusion. In Fig. 12c, the diffusion of E3 in M5 and M6 is similar, higher than that in M7, because the carbon crosslinks in the former two shape the structural pores more than the latter. As shown in Fig. 12d, for the same reason, the diffusivity of E4 in M6 is greater than in M7. The diffusivity of E4 in M4 is less than M6, mainly since M6 has more chain scissions and the concentration of E4 in it is smaller. As Fig. 12e shows, the diffusion of E5 in M7 is greater than that of M8 and M9, which is attributed to more chain scissions and fewer crosslinks, resulting in more free chains. Comparing M8 to M9, the former has a slightly higher diffusion rate than the latter because the concentration of E5 in the former is smaller.

Depending on the above analysis, the relaxation of EPDM with self-diffusion as its proxy, is mainly related to free chain, crosslinking, and concentration. Chain scissions will increase the free chains in the system, which can further promote the movement of molecular segments, while crosslinking will inhibit the diffusion of molecular chains. Carbon crosslinking has a slightly less restrictive effect on molecular diffusion than ether crosslinking, because the radius of gyration is larger than that of the ether crosslinking, providing more free volume for diffusion. It can be inferred that the relaxation properties of EPDM will first increase with the formation of chain scission, and then decrease with the formation of ether crosslinks during degradation. Moreover, the concentration of molecules in the system also limits diffusion.

3.3 Glass-transition temperature

As shown in Fig. 13, the calculated glass transition temperatures of the nine EPDM models which are listed in Table 2 (p.510) are between 238 and 272 K. In Fig. 13a, M3 has the highest glass transition temperature, followed by M2 and M1. It can be concluded that crosslinking reduces molecular motion

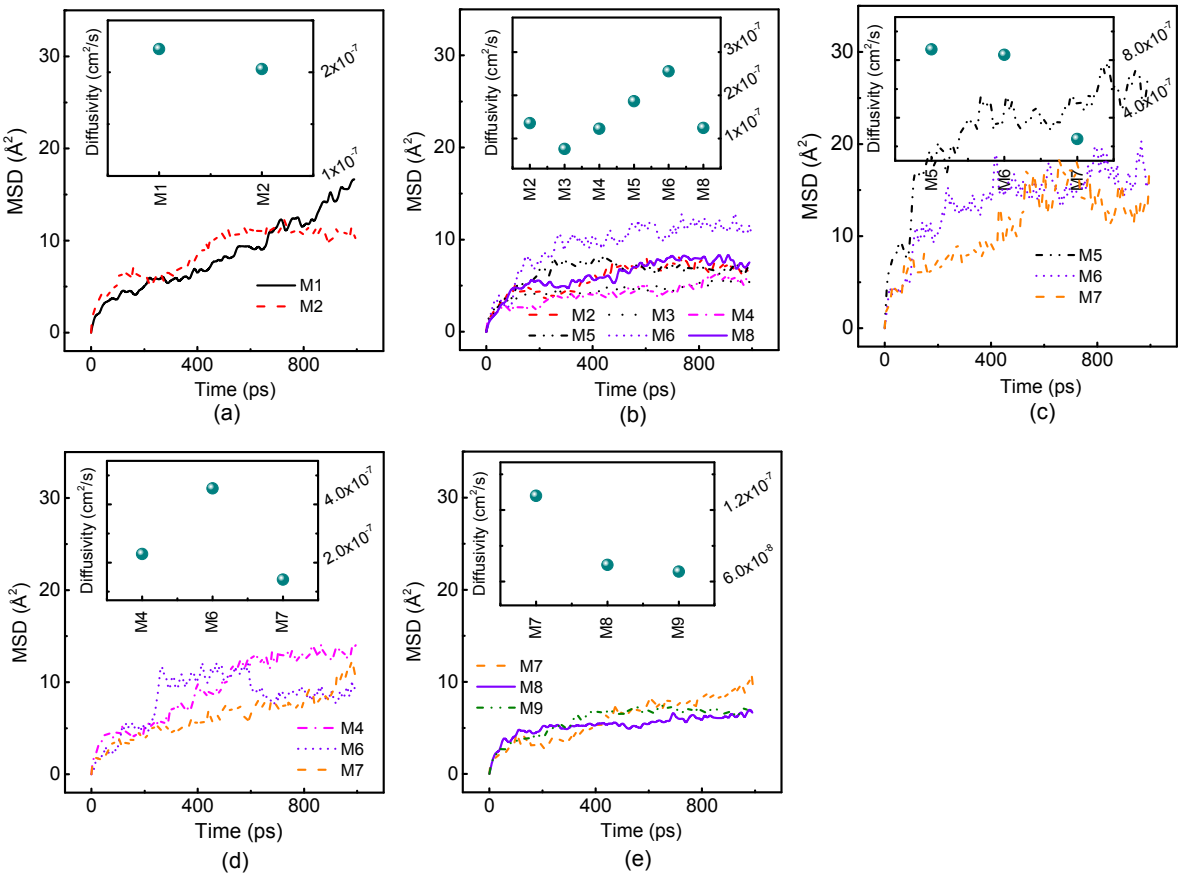

Fig. 12 MSD and self-diffusivity of various EPDM molecular chains of E1, E2, E3, E4, and E5 in thermo-oxidative systems

(a) Diffusion of E1 in its constituent models M1 and M2; (b) Self-diffusion of E2 in M2, M3, M4, M5, M6, and M8; (c) Self-diffusion of E3 in M5, M6, and M7; (d) Self-diffusion of E4 in M4, M6, and M7; (e) Self-diffusion of E5 in M7, M8, and M9

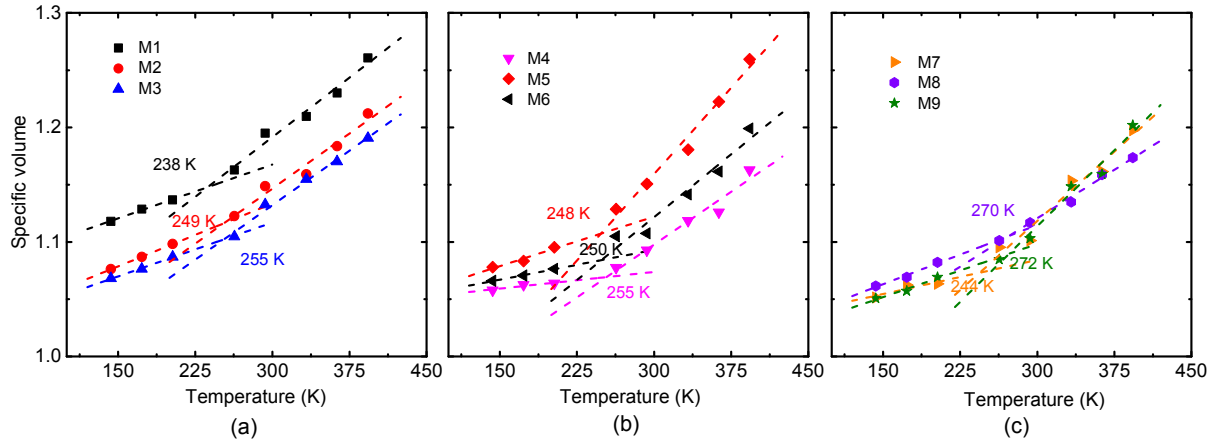

Fig. 13 Variation of the specific volume of EPDM thermo-oxidative models with varying temperatures of 148, 178, 208, 268, 298, 333, 363, and 393 K

(a) Intersections of the fitted curves correspond to the glass transition temperatures. The glass transition temperatures of M1, M2, and M3 are 238, 249, and 255 K, respectively; (b) The glass transition temperatures of M4, M5, and M6 are 255, 248, and 250 K, respectively; (c) The glass transition temperatures of M7, M8, and M9 are 244, 270, and 272 K, respectively

and raises the glass transition temperature. In Fig. 13b, M5 has the lowest glass transition temperature, followed by M6 and M4, which is in agreement with M5 having the most scissions, and the least hydroxyl groups, also followed by M6 and M4. The reason is mainly due to the differences in the number of chain scissions contained and to polarity. In Fig. 13c, the number of crosslinks of M7 is less than that of M8 and M9, so the glass transition temperature of M7 is the smallest, and the difference between M8 and M9 is that the crosslink age of M8 consists of ether crosslinks and carbon crosslinks, while in M9 all crosslinks are ether.

It can therefore be concluded that the glass transition temperature is affected by the number of crosslinks and free chains, the crosslinking type, and the polarity, where crosslinking would raise T_g, while free chains (especially broken chains) lower T_g, and polarity can be seen as weakened crosslinking and therefore also raises T_g. Besides, ether crosslinking has a more profound effect on the glass transition temperature than carbon crosslinking because of its weak polarity. However, due to the coupling of polarity and crosslinking, it is hard to compare the effects of the crosslinking type and the amount of crosslinking as well as chain scissions on the glass transition in this study.

Table 2 Simulation results of the glass transition temperatures for nine MD models of EPDM

Model	Component	T_g (K)
M1	100% HFC	238
M2	50% HFC+50% CCL	249
M3	100% CCL	255
M4	50% CCL+50% HC	255
M5	50% CCL+50% CS	248
M6	50% CCL+25% CS+25% HC	250
M7	25% CS+25% HC+50% ECL	244
M8	50% CCL+50% ECL	270
M9	100% ECL	272

3.4 Uniaxial mechanical properties

Fig. 14 shows the uniaxial compressive stress-strain curves of each model, and the slope of the curve represents the compressive modulus. Since an all-atom simulation limits the larger system that can clearly show structural differences, the resulting difference in the stress-strain relationship for each model can be observed only when the strain is large. As shown in Fig. 14a, the slope of M3 is the largest, followed by M2 and M1, because the number of cross-links decreases in turn. In Fig. 14b, the slopes of M4, M5, and M6 are almost equal, the slopes of the three curves are ordered from large to small, M5>M6>M4, and the number of hydroxyl groups is also reduced in this order. This is because the polarity reduces the entanglement of the molecular chain and weakens the topological constraint among the segments. Slopes of M8 and M9 in Fig. 14c are larger than that of M7 because there are more crosslinks. M8 is slightly larger than M9 because the binding of carbon crosslinks (C-C) in M8 is stronger than that of ether crosslinks (C-O-C) in M9.

4 Conclusions

To understand the fundamentals associated with EPDM's degradation behavior, several EPDM thermo-oxidative models consisting of hydrocarbon chains, carbon crosslinks, chain scissions, hydroxyl chains, and ether crosslinks in different proportions were built. The oxygen diffusivity, glass transition temperature, and stress-strain relationship were measured to verify these thermo-oxidative EPDM models by comparing them with reported experimental results. Then the radius of gyration, free volume, density, transport properties, glass transition, and uniaxial compression performance during degradation were investigated based on valid MD models. The main conclusions were drawn as follows:

1. The radius of gyration contributes decisively to the free volume. The carbon crosslinks (C-C) of EPDM cause the largest radius of gyration, followed by ether crosslinks (C-O-C), hydrocarbon free chains, hydroxyl chains, and chain scissions. Therefore, as the crosslink bonds break and the hydroxyl and chain scissions increase, the free volume and associated viscoelasticity of EPDM decrease during degradation.

2. Although crosslinking creates more free volume to provide space for diffusion, it restricts molecular mobility, so it is negative for diffusion, while free chain increases chain mobility and promotes self-diffusion and oxygen diffusion. The diffusion is also related to the density of the solute. With the thermal oxidation of EPDM, the increase in the

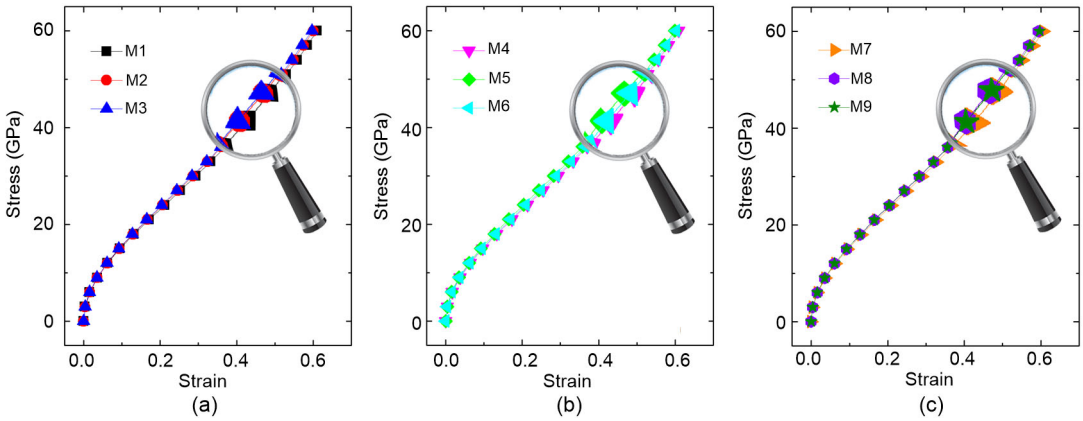

Fig. 14 Uniaxial compressive stress-strain relationships of EPDM thermo-oxidative MD models
The stress-strain curves of M1, M2, and M3 (a), M4, M5, and M6 (b), and M7, M8, and M9 (c)

concentration of oxygen inhibits diffusion and further inhibits ageing.

3. The glass transition temperature reflects the movement ability of the molecular segment and is increased by crosslinking and reduced by free chain and scission. The type of crosslinking has no noteworthy effect on the glass transition temperature of EPDM.

4. The uniaxial compression performance of EPDM mainly depends on the degree of crosslinking, with a higher density of crosslinking resulting in a stronger modulus. In addition, the hydroxyl group weakens the topological constraint caused by entanglement due to its polarity, leading to a decrease in modulus. Therefore, the modulus of EPDM may first decrease in the medium-term from thermal oxidation due to hydroxyl groups and chain scission, and recover in the later stage due to ether crosslinking. Nevertheless, the crosslinking of ether is weaker than that of carbon crosslinking, resulting in a lower modulus than originally.

Contributors

Ya-jian WANG designed the research. Ya-jian WANG and Yu-you YANG processed the corresponding data. Ya-jian WANG wrote the first draft of the manuscript. Yu-you YANG helped to organize the manuscript. Lin-bing WANG revised and edited the final version.

Conflict of interest

Ya-jian WANG, Yu-you YANG, and Lin-bing WANG declare that they have no conflict of interest.

References

Assink RA, Gillen KT, Sanderson B, 2002. Monitoring the degradation of a thermally aged EPDM terpolymer by ^{1}H NMR relaxation measurements of solvent swelled samples. *Polymer*, 43(4):1349-1355. https://doi.org/10.1016/S0032-3861(01)00661-9

Banik I, Bhowmick AK, 2000. Effect of electron beam irradiation on the properties of crosslinked rubbers. *Radiation Physics and Chemistry*, 58(3):293-298. https://doi.org/10.1016/S0969-806X(99)00371-0

Bouguedad D, Mekhaldi A, Boubakeur, Ahmed, et al., 2008. Thermal ageing effects on the properties of ethylene-propylene-diene monomer (EPDM). *Annales de Chimie (Paris 1914)*, 33(4):303-313.

Cao H, Gu Z, Chen Z, et al., 2016. Sub-rouse mode relaxation in ethylene-propylene-diene rubber above glass transition. *Acta Polymerica Sinica*, (9):1206-1211 (in Chinese). https://doi.org/10.11777/j.issn1000-3304.2016.15379

Charati SG, Stern SA, 1998. Diffusion of gases in silicone polymers: molecular dynamics simulations. *Macromolecules*, 31(16):5529-5535. https://doi.org/10.1021/ma980387e

Choi SS, Jose J, Lyu MY, et al., 2010. Influence of filler and cure systems on thermal aging resistance of natural rubber vulcanizates under strained condition. *Journal of Applied Polymer Science*, 118(5):3074-3081. https://doi.org/10.1002/app.32738

Colin X, Hassine MB, Nait-Abelaziz M, 2019. Chemo-mechanical model for predicting the lifetime of EPDM rubbers. *Rubber Chemistry and Technology*, 92(4):722-748. https://doi.org/10.5254/rct.19.81469

Cui T, Chao YJ, van Zee JW, 2012. Stress relaxation behavior of EPDM seals in polymer electrolyte membrane fuel cell environment. *International Journal of Hydrogen Energy*, 37(18):13478-13483. https://doi.org/10.1016/j.ijhydene.2012.06.098

Delor F, Teissedre G, Baba M, et al., 1998. Ageing of

EPDM—2. Role of hydroperoxides in photo-and thermo-oxidation. *Polymer Degradation and Stability*, 60(2-3): 321-331.
https://doi.org/10.1016/S0141-3910(97)00087-6

Delor-Jestin F, Lacoste J, Barrois-Oudin N, et al., 2000. Photo-, thermal and natural ageing of ethylene–propylene–diene monomer (EPDM) rubber used in automotive applications. Influence of carbon black, crosslinking and stabilizing agents. *Polymer Degradation and Stability*, 67(3):469-477.
https://doi.org/10.1016/S0141-3910(99)00147-0

Duek ER, Juliano VF, Guzzo M, et al., 1990. The photo-oxidation of EPDM rubber: part II—the photo-initiation process. *Polymer Degradation and Stability*, 28(3):235-248.
https://doi.org/10.1016/0141-3910(90)90066-G

Ferradino AG, 2003. Antioxidant selection for peroxide cure elastomer applications. *Rubber Chemistry and Technology*, 76(3):694-718.
https://doi.org/10.5254/1.3547763

Ghasemi M, Morteza SM, 2013. Performance improvement of a crumb rubber modified bitumen using recycled glass powder. *Journal of Zhejiang University-SCIENCE A (Applied Physics & Engineering)*, 14(11):805-814.
http://doi.org/10.1631/jzus.A1300053

Gorur RS, Rajan SS, Amburgey OG, 1989. Contamination performance of polymeric insulating materials used for outdoor insulation applications. *IEEE Transactions on Electrical Insulation*, 24(4):713-716.
https://doi.org/10.1109/14.34207

Gu Z, Zhang X, Bao C, et al., 2015. Crosslinking-dependent relaxation dynamics in ethylene-propylene-diene (EPDM) terpolymer above the glass transition temperature. *Journal of Macromolecular Science, Part B*, 54(5): 618-627.
https://doi.org/10.1080/00222348.2015.1018438

Guzzo M, de Paoli MA, 1992. The photo-oxidation of EPDM rubber: part IV—degradation and stabilization of vulcanizates. *Polymer Degradation and Stability*, 36(2):169-172.
https://doi.org/10.1016/0141-3910(92)90153-V

Jiang J, Chen X, Xu JS, et al., 2017. Quasi-static compression mechanical properties of EPDM material after pyrolysis. *Journal of Aerospace Power*, 32(1):114-119 (in Chinese).
https://doi.org/10.13224/j.cnki.jasp.2017.01.016

Landi VR, Easterbrook EK, 1978. Scission and crosslinking during oxidation of peroxide cured EPDM. *Polymer Engineering and Science*, 18(15):1135-1143.
https://doi.org/10.1002/pen.760181503

Li RJ, Corripio AB, Henson MA, et al., 2004. On-line state and parameter estimation of EPDM polymerization reactors using a hierarchical extended Kalman filter. *Journal of Process Control*, 14(8):837-852.
https://doi.org/10.1016/j.jprocont.2004.03.002

Lim SY, Sahimi M, Tsotsis TT, et al., 2007. Molecular dynamics simulation of diffusion of gases in a carbon-nanotube–polymer composite. *Physical Review E*, 76(1): 011810.
https://doi.org/10.1103/PhysRevE.76.011810

Liu Y, Zhou HB, 2016. Analysis of leakage paths induced by longitudinal differential settlement of the shield-driven tunneling. Proceedings of the 3rd International Conference on Engineering Technology and Application, p.914-919.
https://doi.org/10.12783/dtetr/iceta2016/7107

Lucas P, Baba M, Lacoste J, et al., 2002. Crosslinking of dienic elastomers resulting from ageing: X-ray diffraction and refractometry measurements. *Polymer Degradation and Stability*, 76(3):449-453.
https://doi.org/10.1016/S0141-3910(02)00048-4

Ma LX, Yang G, Tang YZ, 2013. The effect of AIREBO on thermal conductivity of EPDM networks. *Key Engineering Materials*, 561:164-168.
https://doi.org/10.4028/www.scientific.net/KEM.561.164

Madkour TM, 2000. Development of the molecular design rules of ultra-permeable poly [1-(trimethylsilyl)-1-propyne] membranes. *Polymer*, 41(20):7489-7497.
https://doi.org/10.1016/s0032-3861(00)00083-5

Moreno VM, Gorur RS, 2001. Effect of long-term corona on non-ceramic outdoor insulator housing materials. *IEEE Transactions on Dielectrics and Electrical Insulation*, 8(1):117-128.
https://doi.org/10.1109/94.910434

Parameswaranpillai J, Pulikkalparambil H, Sanjay MR, et al., 2019a. Polypropylene/high-density polyethylene based blends and nanocomposites with improved toughness. *Materials Research Express*, 6(7):075334.
https://doi.org/10.1088/2053-1591/ab18cd

Parameswaranpillai J, Elamon R, Sanjay MR, et al., 2019b. Synergistic effects of ethylene propylene diene copolymer and carbon nanofiber on the thermo-mechanical properties of polypropylene/high-density polyethylene composites. *Materials Research Express*, 6(8):085302.
https://doi.org/10.1088/2053-1591/ab1d37

Paroli RM, Dutt O, Delgado AH, et al., 1991. Characterization of ethylene-propylene-diene monomer (EPDM) roofing membranes using thermogravimetry and dynamic mechanical analysis. *Thermochimica Acta*, 182(2):303-317.
https://doi.org/10.1016/0040-6031(91)80014-a

Redline EM, Celina MC, Harris CE, et al., 2017. Anomalous aging of EPDM and FEPM under combined thermo-oxidative and hydrolytic conditions. *Polymer Degradation and Stability*, 146:317-326.
https://doi.org/10.1016/j.polymdegradstab.2017.09.010

Rivaton A, Cambon S, Gardette JL, 2004. Radiochemical aging of ethylene–propylene–diene monomer elastomers. I. Mechanism of degradation under inert atmosphere. *Journal of Polymer Science Part A: Polymer Chemistry*, 42(5):1239-1248.
https://doi.org/10.1002/pola.11095

Rivaton A, Cambon S, Gardette JL, 2006. Radiochemical ageing of ethylene–propylene–diene elastomers. 4. Evaluation of some anti-oxidants. *Polymer Degradation*

and Stability, 91(1):136-143. https://doi.org/10.1016/j.polymdegradstab.2005.04.018

Rutherford SW, Limmer DT, Smith MG, et al., 2007. Gas transport in ethylene–propylene–diene (EPDM) elastomer: molecular simulation and experimental study. *Polymer*, 48(22):6719-6727. https://doi.org/10.1016/j.polymer.2007.07.020

Schurch M, 2006. Small but important–gasket for tunnel segments. Proceedings of the International Symposium on Underground Excavation and Tunnelling, p.239-248.

Scoponi M, Pradella F, Carassiti V, et al., 1994. Photodegradation of poly [ethylene-*co*-propene-*co*-(5-ethylidene-2-norbornene)] rubbers, 1. Reappraisal of the photooxidation mechanism under accelerated conditions. *Macromolecular Chemistry and Physics*, 195(3):985-997. https://doi.org/10.1002/macp.1994.021950315

Teissedre G, Pilichowski JF, Chmela S, et al., 1996. Ageing of EPDM—I: photo and thermal stability of EPDM hydroperoxides. *Polymer Degradation and Stability*, 53(2):207-215. https://doi.org/10.1016/0141-3910(96)00082-1

Tomer NS, Delor-Jestin F, Singh RP, et al., 2007. Crosslinking assessment after accelerated ageing of ethylene propylene diene monomer rubber. *Polymer Degradation and Stability*, 92(3):457-463. https://doi.org/10.1016/j.polymdegradstab.2006.11.013

Wang WW, Tanaka Y, Takada T, et al., 2018. Influence of oxidation on the dynamics in amorphous ethylene-propylene-diene-monomer copolymer: a molecular dynamics simulation. *Polymer Degradation and Stability*, 147:187-196. https://doi.org/10.1016/j.polymdegradstab.2017.12.001

Wang WZ, Qu BJ, 2003. Photo- and thermo-oxidative degradation of photocrosslinked ethylene–propylene–diene terpolymer. *Polymer Degradation and Stability*, 81(3):531-537. https://doi.org/10.1016/S0141-3910(03)00154-X

Wang YH, Yang G, Wang WH, et al., 2019. Effects of different functional groups in graphene nanofiber on the mechanical property of polyvinyl alcohol composites by the molecular dynamic simulations. *Journal of Molecular Liquids*, 277:261-268. https://doi.org/10.1016/j.molliq.2018.12.089

Wang YJ, Yang YY, Tao MJ, 2019. Understanding free volume characteristics of ethylene-propylene-diene monomer (EPDM) through molecular dynamics simulations. *Materials*, 12(4):612. https://doi.org/10.3390/ma12040612

Wu CF, Xu WJ, 2006. Atomistic molecular modelling of crosslinked epoxy resin. *Polymer*, 47(16):6004-6009. https://doi.org/10.1016/j.polymer.2006.06.025

Wu CF, Xu WJ, 2007. Atomistic simulation study of absorbed water influence on structure and properties of crosslinked epoxy resin. *Polymer*, 48(18):5440-5448. https://doi.org/10.1016/j.polymer.2007.06.038

Wu HN, Huang RQ, Sun WJ, et al., 2014. Leaking behavior of shield tunnels under the Huangpu river of Shanghai with induced hazards. *Natural Hazards*, 70(2):1115-1132. https://doi.org/10.1007/s11069-013-0863-z

Zachary M, Camara S, Whitwood AC, et al., 2008. EPR study of persistent free radicals in cross-linked EPDM rubbers. *European Polymer Journal*, 44(7):2099-2107. https://doi.org/10.1016/j.eurpolymj.2008.04.008